

AD-A074 734

ARMY RESEARCH AND TECHNOLOGY LABS FORT EUSTIS VA
MODEL 540 ROTOR BLADE CRACK PROPAGATION INVESTIGATION.(U)
AUG 79 D E GOOD
USARTL-TR-79-26

F/G 1/3

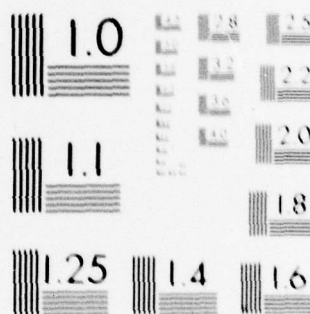
UNCLASSIFIED

NL

| OF |

AD
A074734





MICROCOPY RESOLUTION TEST CHART
NATIONAL BUREAU OF STANDARDS-1963-A

14
USARTL-TR-79-26

12



AD A 074734

LEVEL 4

6 MODEL 540 ROTOR BLADE CRACK PROPAGATION INVESTIGATION

10 Danny E. Good

12 35

DDC
RECEIVED
OCT 8 1979

11 August 1979

16 1F262209AH76

17 00

9 Final Report for Period January 1978 - February 1978

DDC FILE COPY

Jan-Feb '78

Approved for public release;
distribution unlimited.

APPLIED TECHNOLOGY LABORATORY
U. S. ARMY RESEARCH AND TECHNOLOGY LABORATORIES (AVRADCOM)
Fort Eustis, Va. 23604

393742

y/b

79 10 04 041

DISCLAIMERS

The findings in this report are not to be construed as an official Department of the Army position unless so designated by other authorized documents.

When Government drawings, specifications, or other data are used for any purpose other than in connection with a definitely related Government procurement operation, the United States Government thereby incurs no responsibility nor any obligation whatsoever, and the fact that the Government may have formulated, furnished, or in any way supplied the said drawings, specifications, or other data is not to be regarded by implication or otherwise as in any manner licensing the holder or any other person or corporation, or conveying any rights or permission, to manufacture, use, or sell any patented invention that may in any way be related thereto.

Trade names cited in this report do not constitute an official endorsement or approval of the use of such commercial hardware or software.

DISPOSITION INSTRUCTIONS

Destroy this report when no longer needed. Do not return it to the originator.

Unclassified

SECURITY CLASSIFICATION OF THIS PAGE (When Data Entered)


REPORT DOCUMENTATION PAGE		READ INSTRUCTIONS BEFORE COMPLETING FORM
1. REPORT NUMBER USARTL TR 79 26	2. GOVT ACCESSION NO.	3. RECIPIENT'S CATALOG NUMBER
4. TITLE (and Subtitle) MODEL 540 ROTOR BLADE CRACK PROPAGATION INVESTIGATION		5. TYPE OF REPORT & PERIOD COVERED Final Report January 1978 - February 1978
7. AUTHOR(s) Danny E. Good		6. PERFORMING ORG. REPORT NUMBER
9. PERFORMING ORGANIZATION NAME AND ADDRESS Applied Technology Laboratory, U.S. Army Research and Technology Laboratories (AVRADCOM) Fort Eustis, Virginia 23604		8. CONTRACT OR GRANT NUMBER(s) House Task 79-11
11. CONTROLLING OFFICE NAME AND ADDRESS		10. PROGRAM ELEMENT, PROJECT, TASK AREA & WORK UNIT NUMBERS 62209A 1F262209AH76 00 020 EK
13. MONITORING AGENCY NAME & ADDRESS (if different from Controlling Office)		12. REPORT DATE August 1979
		13. NUMBER OF PAGES 34
		14. SECURITY CLASS. (of this report) Unclassified
16. DISTRIBUTION STATEMENT (of this Report) Approved for public release; distribution unlimited.		15. DECLASSIFICATION/DOWNGRADING SCHEDULE
17. DISTRIBUTION STATEMENT (of the abstract entered in Block 20, if different from Report)		
18. SUPPLEMENTARY NOTES		
19. KEY WORDS (Continue on reverse side if necessary and identify by block number) Helicopters Ammunition Damage Fatigue Tests (Mechanics) Rotor Blades Crack Propagation AH-1		
20. ABSTRACT (Continue on reverse side if necessary and identify by block number) → The rate of crack propagation from an induced defect in a metal Bell Helicopter 540 main rotor blade was investigated. A controlled crack front was introduced into the top surface of the blade spar. Fatigue testing was conducted at maximum level flight loads and the crack growth was monitored. Experimental data was then compared with analytical predictions to measure the ability to predict crack growth characteristics.		

Unclassified

SECURITY CLASSIFICATION OF THIS PAGE (When Data Entered)

TABLE OF CONTENTS

	<u>Page</u>
LIST OF ILLUSTRATIONS	4
INTRODUCTION	5
TEST SPECIMEN CONFIGURATION.....	6
TEST EQUIPMENT	8
TEST LOAD DETERMINATION	10
CRACK GROWTH PREDICTIONS	11
TEST PROCEDURE	17
TEST RESULTS	18
CONCLUSIONS.....	25
LIST OF REFERENCES	26
 APPENDIXES	
A - Crack Propagation Calculations	27
B - Test Load and Crack Growth Record.....	28
C - Scanning Electron Fractographs of Fracture Surface of 540 Rotor Blade Spar	30
LIST OF SYMBOLS.....	34

Accession For	
NTIS GRA&I	<input checked="checked" type="checkbox"/>
DDC TAB	<input type="checkbox"/>
Unannounced	
Justification	
By _____	
Distribution/ _____	
Availability Codes	
Dist	Avail and/or special
	

LIST OF ILLUSTRATIONS

<u>Figure</u>		<u>Page</u>
1	Cross section of 540 rotor blade	6
2	Modified 540 rotor blade for testing	7
3	540 rotor blade spar geometry at Station 154.....	7
4	Fatigue test machine-load application	9
5	Geometry of central crack in an infinite plate.....	12
6	Stress-intensity-factor coefficient for a single crack emanating from a circular hole in a uniaxial stress state	14
7	Correction factor for eccentricity and finite width.....	15
8	Idealized rotor blade test specimen geometry	16
9	Actual crack length versus number of applied cycles.....	20
10	Effective half-crack length versus number of applied cycles	21
11	Crack propagation rate versus stress-intensity-factor range	22
12	Crack propagation rate versus stress-intensity-factor range	23
13	Sectioned spar after test	24

INTRODUCTION

This program was undertaken as a portion of an overall effort to investigate the effects of ballistic damage on a variety of metal and composite rotor blades. When a rotor blade spar is subjected to ballistic impact, the resulting damage is generally an irregularly shaped hole with many sharp edges that produce stress concentrations. Normally, one sharp edge will produce the most critical stress concentration. It is from this point that the first fatigue crack will initiate and propagate. The objective of this program was to investigate, through analysis and test, the rate of crack propagation in a metal blade spar from an induced defect. The rotor blade evaluated in this program was a Bell Helicopter Company (BHC) 540 main rotor blade. A 3/4-inch-diameter hole with a saw cut that was stop drilled to produce a controlled crack front was introduced into the top surface of the blade spar. The blade was fatigue tested to initiate a crack. Fatigue testing was continued at maximum level flight loads and the crack growth was monitored. The experimental data was then compared with analytical predictions to obtain a measure of the ability to predict the crack growth characteristics.

TEST SPECIMEN CONFIGURATION

The rotor blade tested was a Bell Helicopter Company (BHC) Model 540 main rotor blade and was residual property from the Model 540 Rotor Blade Fatigue Test Program (Reference 1). The blade is approximately 19 feet long with a 27-inch chord and a 9-1/3-percent-thick symmetrical airfoil section. Figure 1 shows a typical cross section of the 540 rotor blade. The spar is made from a C-section extrusion of 2024 aluminum alloy and forms the basic profile of the leading edge. The spar spacer is also a 2024 aluminum alloy extrusion and when bonded in place controls the airfoil thickness. The blade from the spar aft is composed of aluminum honeycomb core and skins bonded to the spar. The trailing edge is a strip of extruded aluminum. The spar and trailing edge strip are tapered between Stations 80 and 140 (see Figure 2) and are of constant chord outboard of Station 140.

The tip end of the blade was modified by BHC for testing purposes. A 22-inch section of the tip was removed and a stepped aluminum doubler was installed (see Figure 2).

The blade test specimen had been previously used for the fatigue test evaluation and investigation of the spar spacer, which had partially debonded from the spar during that testing. Station 154 was selected as the test section for this test because the debond of the spacer had propagated at least 12 inches inboard and outboard of Station 154. This precluded propagation of the debond through the test section, thus eliminating a potential unknown variable in the test conditions.

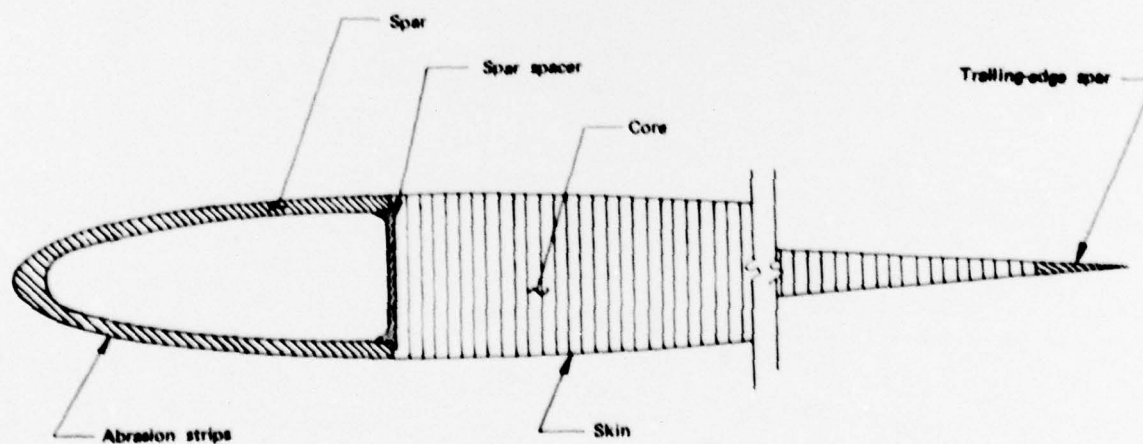


Figure 1. Cross section of 540 rotor blade.

¹Gustafson, A. J., and Calapodas, N. J., *Model 540 Rotor Blade Fatigue Test*, USAAMRDL Technical Note 22, Eustis Directorate, U.S. Army Air Mobility Research and Development Laboratory, Fort Eustis, Virginia, January 1976, AD A021472.

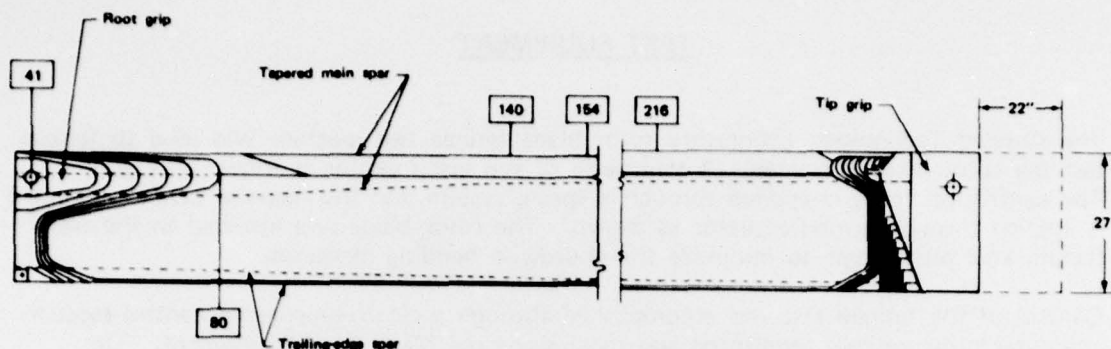


Figure 2. Modified 540 rotor blade for testing.

A 3/4-inch-diameter hole was counterbored in the top side of the blade at Station 154. A chordwise saw cut 0.10 inch in length was made from the hole toward the leading edge of the blade. A 1/64-inch hole was drilled at the tip of the saw cut to produce a controlled crack tip front. The geometry of the induced defect in the blade is shown in Figure 3.

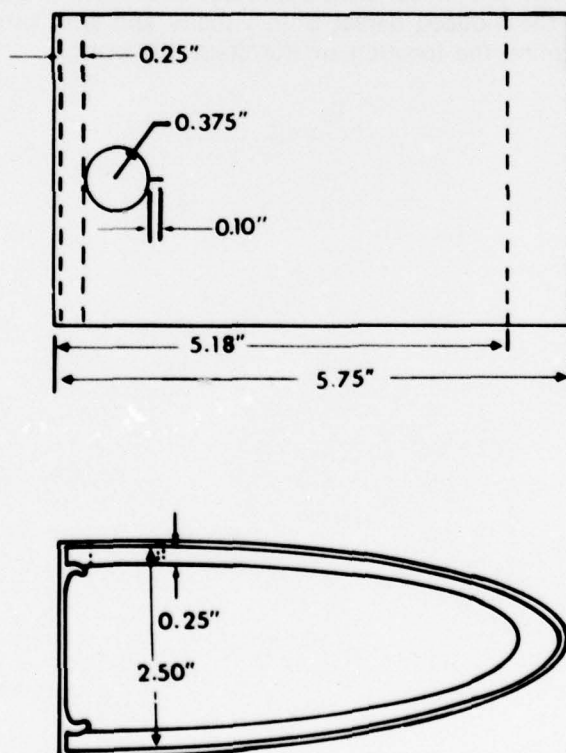


Figure 3. 540 rotor blade spar geometry at Station 154.

TEST EQUIPMENT

The Applied Technology Laboratory rotor blade fatigue test machine was used to fatigue test the rotor blade specimen. A schematic of the test machine is shown in Figure 4. The centrifugal force is applied through a spring system and the flapwise bending moment is applied through a load actuator as shown. The rotor blade was installed in the test fixture at a pitch angle to minimize the chordwise bending moments.

Control of the fatigue test was accomplished through a closed-loop servo control system computer program that monitored and maintained the blade bending moment. The resonant frequency was found by manually adjusting the frequency up and down in 0.005 Hz increments and was then maintained automatically.

The blade test specimen used the same instrumentation as in the previous testing, as discussed in Reference 1. The moments and strains developed in the blade were sensed by the strain gages and were recorded. Data acquisition was initiated systematically by the control system computer at the beginning of each 10,000-cycle block of constant amplitude load cycles.

After completion of each segment of constant amplitude load cycles, the spar was inspected in the region of the induced defect both visually and with ultrasonic shear-wave transmission to determine the location of the crack tip front.

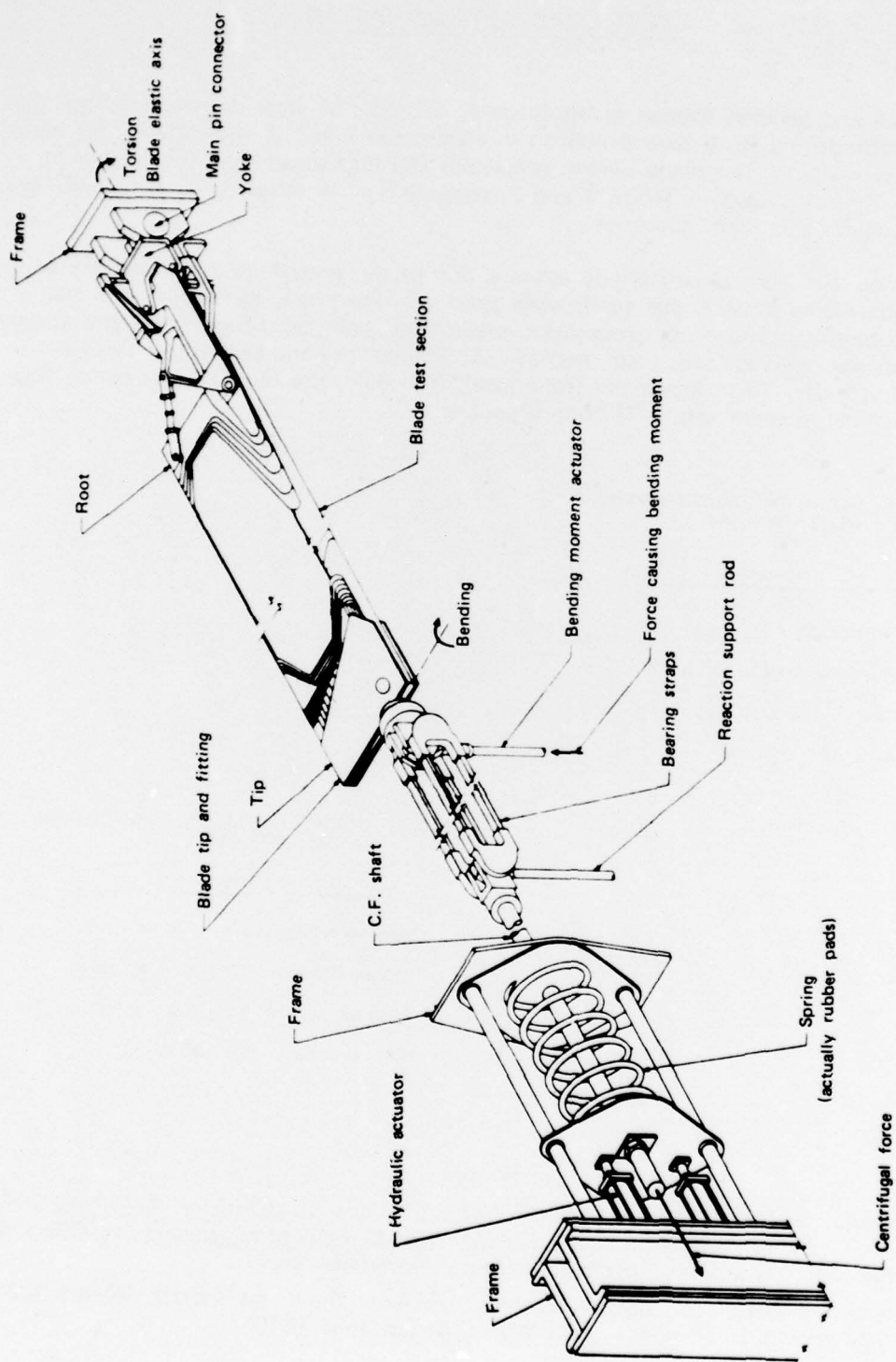


Figure 4. Fatigue test machine-load application.

TEST LOAD DETERMINATION

The axial and bending stresses in the blade at Station 154 were determined from the blade stiffness and loads data contained in References 2 and 3, respectively, for high-speed level flight. The blade section properties and high-speed level flight loads at Station 154 are shown in Tables 1 and 2, respectively. A stress ratio, $R = 0.74$, was calculated for this flight condition.

At Station 154 the primary steady stress is due to the centrifugal force and the primary alternating stress is due to flapwise bending. Therefore, to simplify the test loading condition and crack propagation predictions, only centrifugal force and alternating flapwise bending loads were applied. At Station 154 the centrifugal force is 76,000 pounds. To maintain the stress ratio, $R = 0.74$, the required alternating flapwise bending moment was ± 7500 inch-pounds.

TABLE 1. BLADE STIFFNESS PROPERTIES
AT STATION 154

STIFFNESS
Flapwise, 35×10^6 lb-in. ²
Chordwise, 3060×10^6 lb-in. ²
Torsion, 33.8×10^6 lb-in. ²
Axial, 42.5×10^6 lb

TABLE 2. HIGH-SPEED LEVEL FLIGHT LOADS
AT STATION 154

LOAD
Flapwise bending, $-3 \pm 7.7 \times 10^3$ in.-lb
Chordwise bending, $88 \pm 26 \times 10^3$ in.-lb
Torsional moment, $2.2 \pm 5.5 \times 10^3$ in.-lb
Centrifugal force, 76×10^3 lb

²Structural Analysis of 540-011-100-13 Hub and Blade Assembly for the Model 209/AH-1J, UH-1C, UH-1E, AH-1G, UH-1L, UH-1M, HH-1K Helicopters, Report 209-099-174, Bell Helicopter Company, Fort Worth, Texas, November 1969.

³Qualification Load Level Survey for Improved Main Rotor for AH-1G, Report 209-099-305, Bell Helicopter Company, Fort Worth, Texas, June 1970.

CRACK GROWTH PREDICTIONS

The crack growth predictions were made using Forman's Equation (Reference 4) where the crack propagation rate is a function of the stress-intensity-factor range, ΔK , and the stress ratio, R , as follows:

$$\frac{da}{dN} = \frac{C (\Delta K)^n}{(1-R)K_c - \Delta K} \quad (1)$$

In general, the stress-intensity factor, K , is a function of the maximum stress level, σ , and the half-crack length, a :

$$K = \sigma \sqrt{\pi a} \quad (2)$$

Likewise, the stress-intensity-factor range, ΔK , is

$$\Delta K = \Delta \sigma \sqrt{\pi a} \quad (3)$$

where

$$\Delta \sigma = (1-R)\sigma \quad (4)$$

For 2024 aluminum, a representative value for n is 3.0. Substituting Equation (3) and Equation (4) into Equation (1) and integrating, the following equation results:

$$N_f - N_o = \frac{2}{\pi C (1-R)^2 \sigma^2} \left[\left(\frac{K_c}{K_o} \right) - \left(\frac{K_c}{K_f} \right) - (\ell n) \left(\frac{K_f}{K_o} \right) \right] \quad (5)$$

Letting $K_f = K_c$,

$$N_c - N_o = \frac{2}{\pi C (1-R)^2 \sigma^2} \left[\left(\frac{K_c}{K_o} \right) - (1) - (\ell n) \left(\frac{K_c}{K_o} \right) \right] \quad (6)$$

The above equations apply to the case of the centrally cracked infinite plate as shown in Figure 5. However, the crack growth under consideration is that of a crack propagating from one side of a hole located eccentrically in a finite-width plate. To treat this case, modifications to the theoretical stress-intensity factors were made using the methodology of Figge and Newman (Reference 5).

⁴Forman, R. O., Kearney, V. E., and Engle, R. M., *Numerical Analysis of Crack Propagation in Cyclic-Loaded Structures*, Journal of Basic Engineering, September 1967.

⁵Figge, I. E., and Newman, J. C., Jr., *Fatigue Crack Propagation in Structures With Simulated Rivet Forces*, ASTM Special Technical Publication No. 415, American Society for Testing and Materials, Philadelphia, Pennsylvania, September 1967.

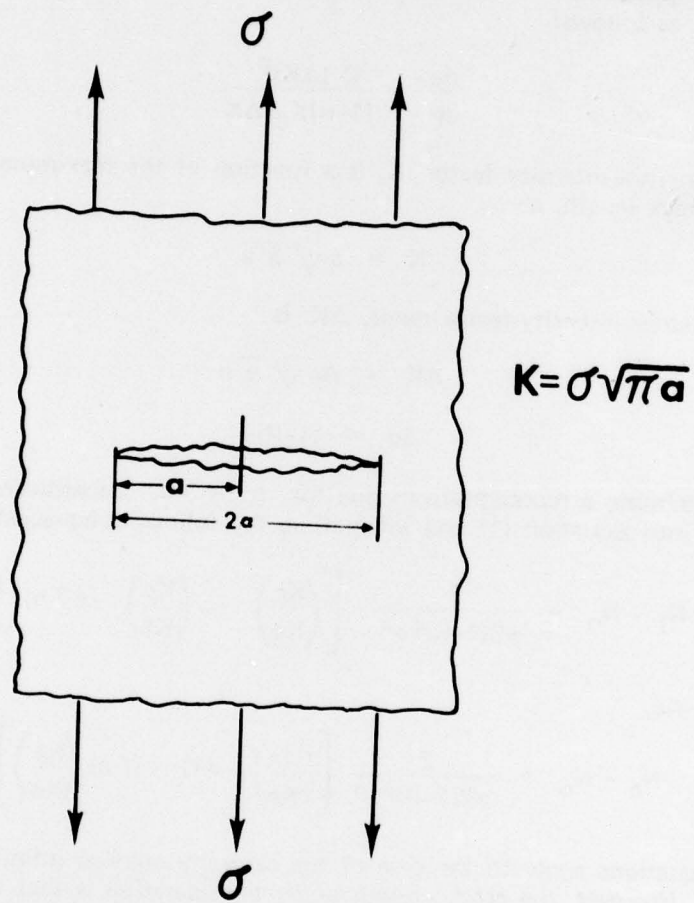


Figure 5. Geometry of central crack in an infinite plate.

In this case, the combination of crack and hole is assumed to be represented by an equivalent crack eccentrically located in an infinite plate. This is accomplished by equating the stress-intensity factors for an infinite plate containing a hole to an infinite plate with a crack. From Reference 6, these stress-intensity factors are, respectively:

$$K = \sigma \sqrt{\pi \ell} f(\ell/r) \quad (7)$$

$$K = \sigma \sqrt{\pi a_e} \quad (8)$$

where the function $f(\ell/r)$ shown in Figure 6 describes the influence of the hole on the stress-intensity factor. Equating these and solving for a_e results in

$$a_e = \ell [f(\ell/r)]^2 \quad (9)$$

The resulting equivalent crack length is found to be nearly equal to 1/2 the sum of the actual crack length and the diameter of the hole.

The stress-intensity factor can be further modified to account for an eccentrically located crack in a finite-width plate as follows:

$$K = \sigma \sqrt{\pi a_e} F(e/b, a_e/b_1) \quad (10)$$

where the function, $F(e/b, a_e/b_1)$, shown in Figure 7, is the boundary correction factor for the eccentrically located crack in a finite-width plate. If Equation (10) is then equated with

$$K = \sigma \sqrt{\pi \bar{a}_e} \quad (11)$$

where \bar{a}_e is the effective half-crack length (taking into account the presence of the hole, eccentricity, and finite width) then

$$\bar{a}_e = \ell f^2(\ell/r) F^2(e/b, a_e/b_1) \quad (12)$$

The rotor blade test specimen geometry was idealized as shown in Figure 8. Appendix A shows the calculated effective half-crack length and resulting crack growth rate and cycles to failure for initial crack lengths, ℓ_0 , varying from 0.25 and 2.75 inches. This calculation uses Equations (1) and (6) respectively, together with the stress-intensity factor of Equation (1). The stress conditions used, which correspond to a centrifugal force of 76,000 pounds and an alternating flapwise bending moment of ± 7500 inch-pounds, are

$$\sigma = 21403 \text{ lb/in.}^2$$

$$\Delta\sigma = 5566 \text{ lb/in.}^2$$

⁶Paris, P. C., and Sih, G.C.M., *Stress Analysis of Cracks*, ASTM Special Technical Publication No. 381, American Society for Testing and Materials, Philadelphia, Pennsylvania, June 1964.

The values of the constants K_C and C determined by Hudson (Reference 7) for 2024 aluminum were selected as representative values for the blade specimen. They are

$$K_C = 100320 \text{ lb/in.}^{3/2}$$

$$C = 3.22 \times 10^{-14}$$

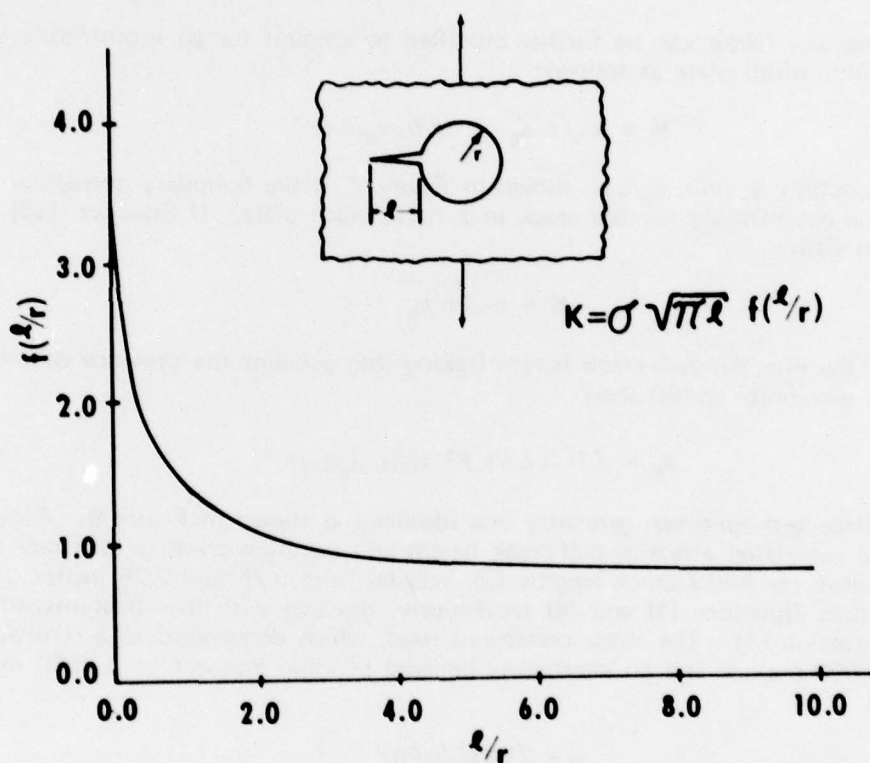


Figure 6. Stress-intensity-factor coefficient for a single crack emanating from a circular hole in a uniaxial stress state.

⁷Hudson, C. M., *Effect of Stress Ratio on Fatigue-Crack Growth in 7075-T6 and 2024-T6 Aluminum-Alloy Specimens*, NASA Technical Note D-5390, National Aeronautics and Space Administration, Washington, D. C., August 1969.

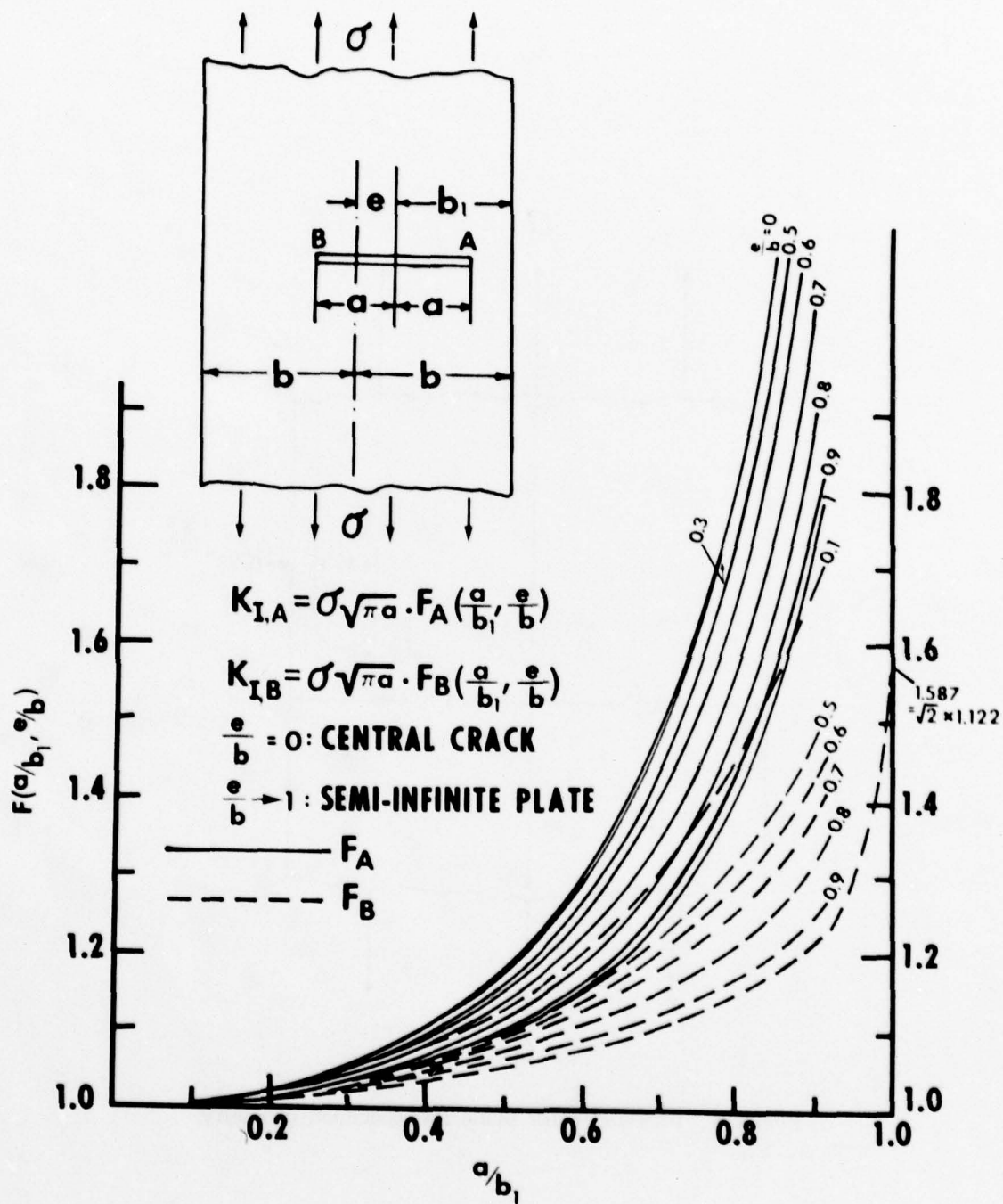


Figure 7. Correction factor for eccentricity and finite width.

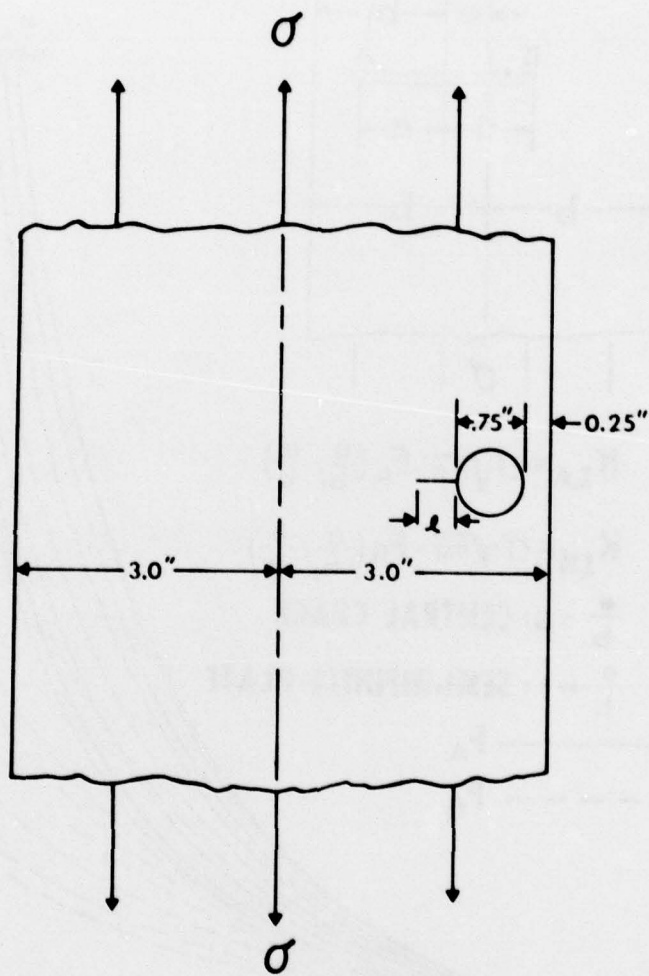


Figure 8. Idealized rotor blade test specimen geometry.

TEST PROCEDURE

The test specimen was installed in the rotor blade test fixture and a steady centrifugal force of 76,000 pounds and an alternating flapwise moment of ± 7500 inch-pounds at Station 154 was applied. The specimen was loaded in blocks of 10,000 cycles each.

Since a crack had not initiated after three load blocks, the alternating flapwise bending moment was increased to $\pm 11,000$ inch-pounds at Station 154 in an attempt to initiate a failure. During this load block a crack initiated and propagated a total of 0.15 inch. The alternating flapwise moment was then reduced to ± 7500 inch-pounds and maintained at that level during each subsequent block of 10,000 load cycles.

The specimen was inspected in the area of the induced effect visually on the outside and on the inside through a mirror system. The crack tip front was located using shear wave ultrasonics and dye penetrant. Once the crack tip front was located, the length of the crack was then measured.

The inspection of the spar was conducted after each block of load cycles through block 16 and then after every other block of load cycles through block 36. The final inspection prior to ultimate failure was made after block 42.

TEST RESULTS

The load history and measured crack length for the test specimen are set forth in Appendix B. The relationship between the actual crack length, ℓ , and the number of applied load cycles is shown in Figure 9, where the initial condition, $N_0 = 0$, is assumed to be the last cycle of load block 4. The corresponding initial crack length, ℓ_0 , is then 0.25 inch.

Using the methodology of the previous selections, the effective half-crack length, \bar{a}_e , was determined for each crack length, ℓ . The resulting relationship between \bar{a}_e and the number of applied load cycles is shown in Figure 10.

The crack propagation rate in the spar was determined using the following methods:

1. A best-fit curve was drawn through the data shown in Figure 10. The slope of the curve was then determined using finite difference techniques. Figure 11 shows the resulting relationship between the crack growth rate, $d\bar{a}_e/dN$, and the stress-intensity-factor range, ΔK . For comparison the crack growth rate, $d\bar{a}_e/dN$, determined using Forman's Equation (Equation 10) is also shown in Figure 11.
2. A best-fit curve was drawn through the data shown in Figure 9. The slope of the curve was determined using finite difference techniques. Figure 12 shows the resulting relationship between the crack growth rate, $d\ell/dN$, and the stress-intensity-factor range, ΔK .
3. The failed spar was sectioned as shown in Figure 13. The fracture surface was examined at the locations shown using the electron scanning microscope at NASA/Langley Research Center. Appendix C shows a series of fractographs of the areas of the fracture surface that was examined.

From the fractographs the fatigue striations were counted and the crack growth rate $d\ell/dN$ was subsequently determined. The resulting crack growth rates are shown in Figure 12.

In each case above, the stress-intensity-factor range is based on the effective half-crack length, \bar{a}_e . Examination of the crack growth rate curves shown in Figure 11 shows a reasonable correlation between the crack growth rate interpolated from the test data and the rate predicted from Forman's Equation.

Examination of the data shown in Figure 12 reveals a similar trend between the crack growth rates determined from the slope of the best-fit curve of Figure 9 and the crack growth rate determined from the striation count. The distinctive characteristic of the data shown in Figure 12 is that the crack growth rate is initially high and then drops off before continuing to increase. Recalling that the crack growth was originally initiated at the higher load level of $\pm 11,000$ inch-pounds and the load was then reduced to ± 7500 inch-pounds, it appears that the phenomenon referred to as "delay retardation" in

Reference 8 occurred. That is to say that the crack growth rate decreased after the higher load/overload cycling. At a point where the crack length, ℓ , had reached approximately 1 inch, the crack growth had resumed a normal crack growth trend.

The "delay retardation" effect does not appear in the crack growth rate versus stress-intensity-factor range shown in Figure 11. This may be a result of the curve smoothing procedure. The lower initial crack growth rate compared to that predicted by Forman's Equation, however, may be due to the "delay retardation" effects. The difference in the slope of the curves shown in Figure 10 may be attributed to variations in the selected material constants C and n .

The critical crack length, ℓ_c , in testing was found to be 4.75 inches based on visual examination of the fracture surface after the test was completed. In comparison, the predicted critical crack length using Forman's Equation was 4.85 inches. The fact that the actual critical length was slightly less than predicted would seem to indicate that the actual critical stress-intensity factor is somewhat less than the representative value selected.

⁸ Hertzberg, R. W., *Deformation and Fracture Mechanics of Engineering Materials*, New York, John Wiley and Sons, 1976.

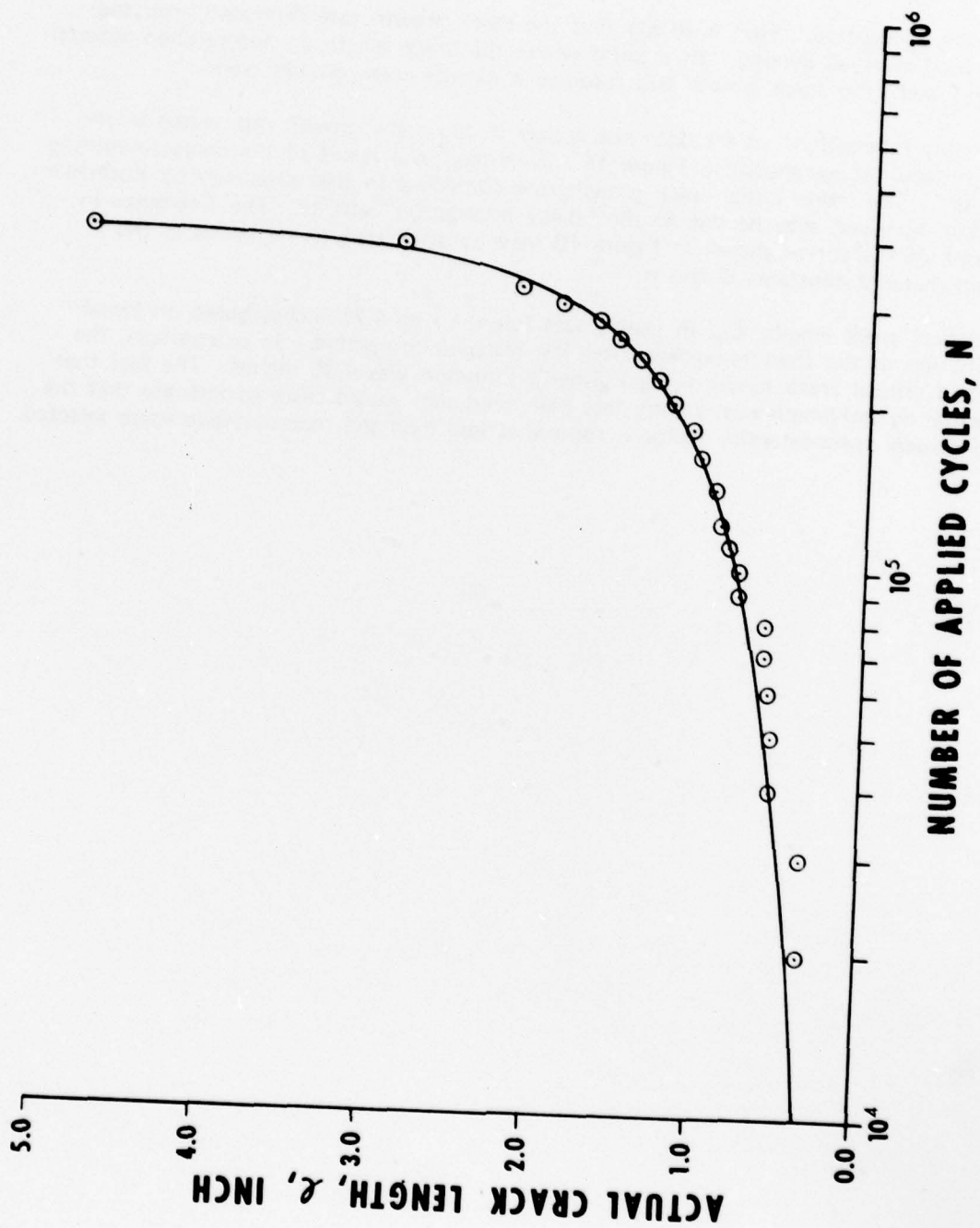


Figure 9. Actual crack length versus number of applied cycles.

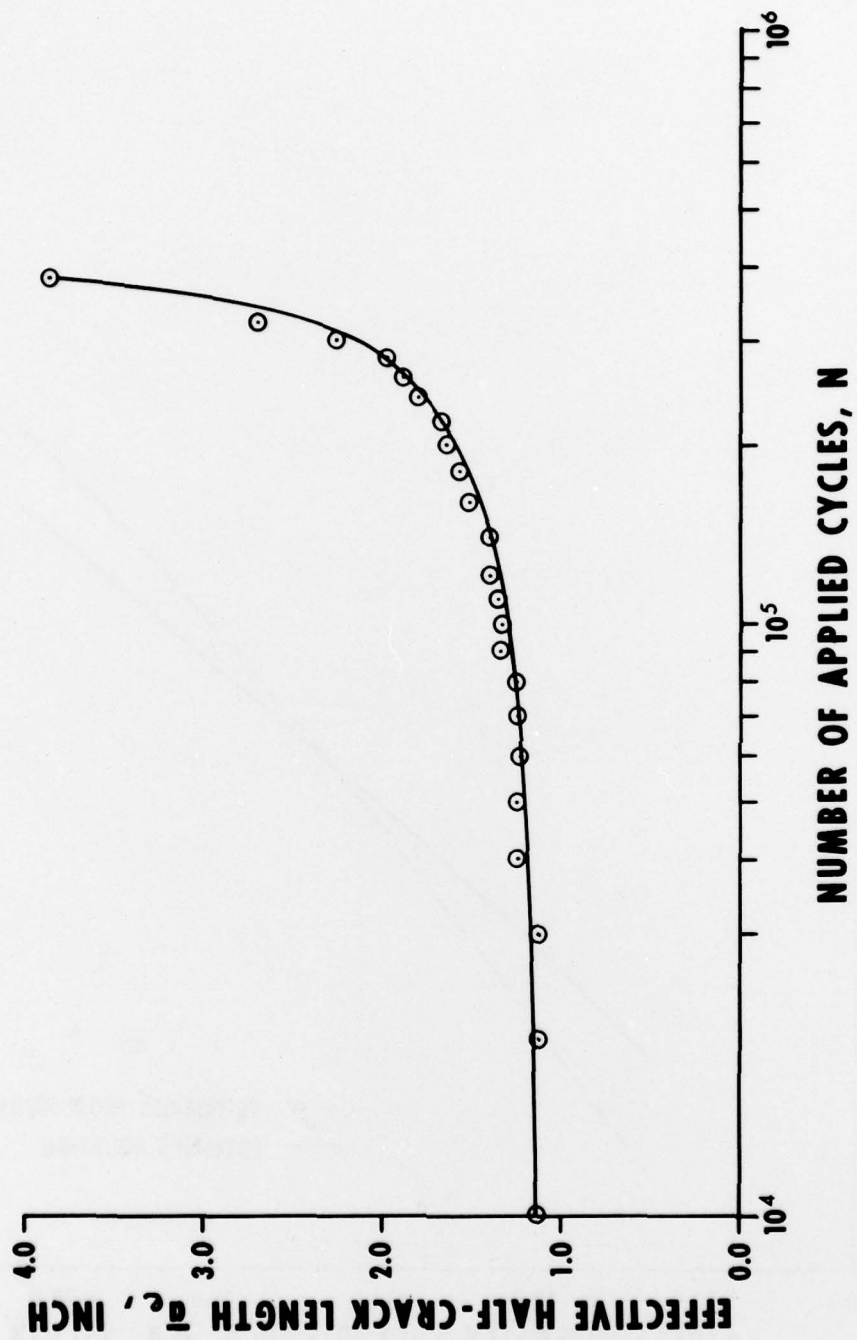


Figure 10. Effective half-crack length versus number of applied cycles.

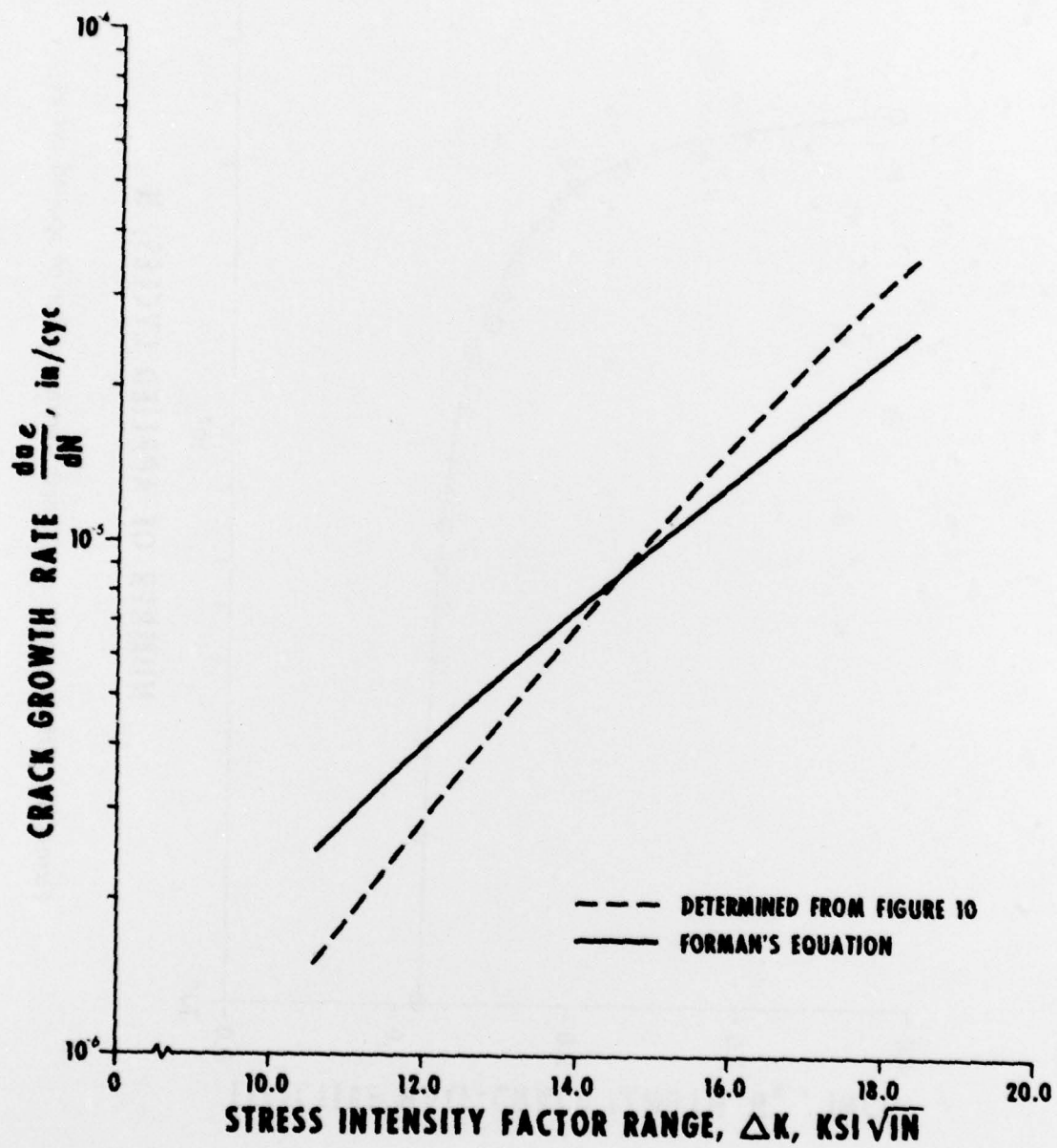


Figure 11. Crack propagation rate versus stress-intensity-factor range.

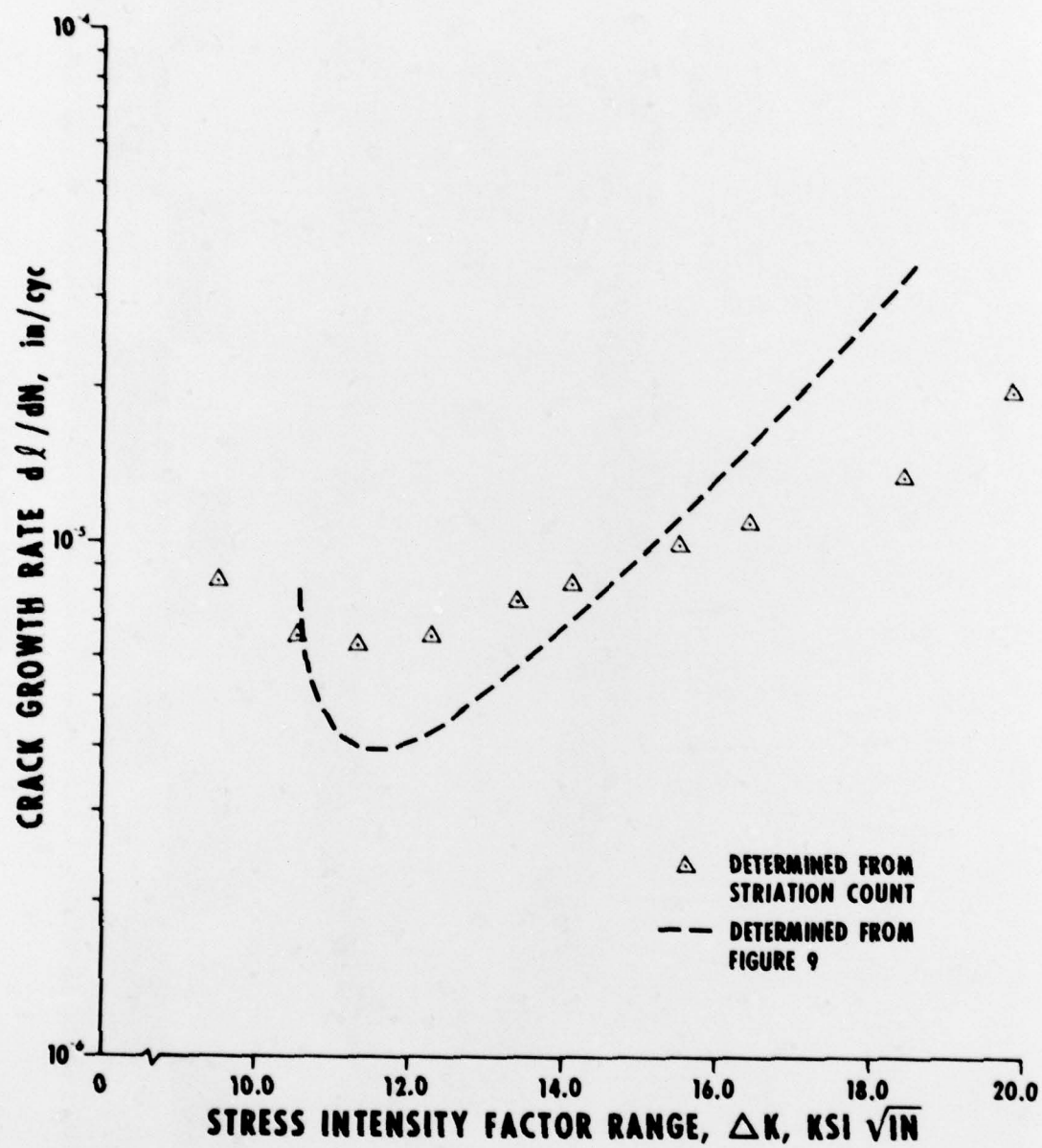


Figure 12. Crack propagation rate versus stress-intensity-factor range.

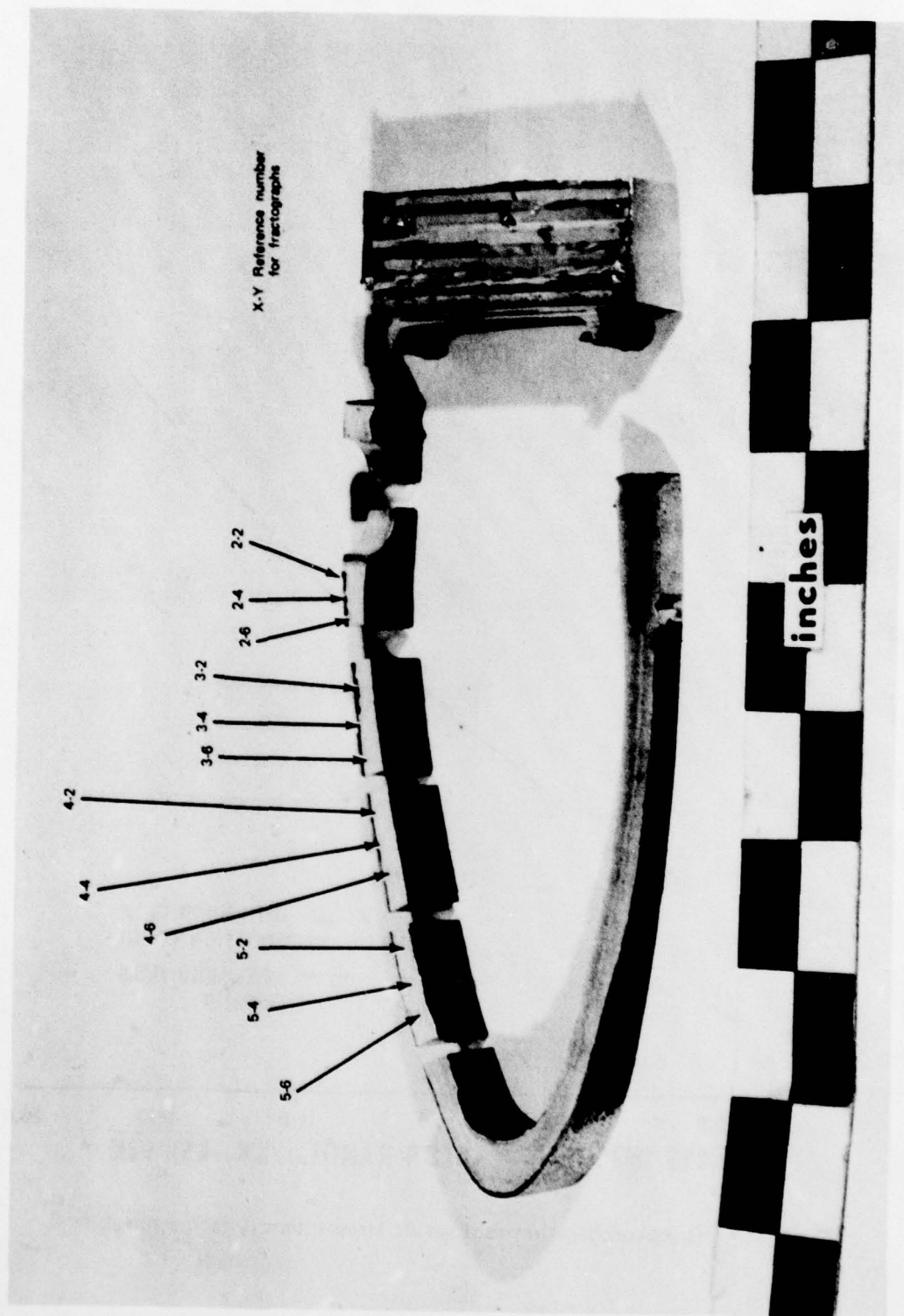


Figure 13. Sectioned spar after test.

CONCLUSIONS

Based on the data obtained from the testing of this single test specimen, it is concluded that:

Forman's Equation can be used to predict the crack growth behavior of a controlled defect in a metal blade spar if the appropriate modifications are made to the stress-intensity factor to incorporate corrections for hole influence, eccentricity, and finite width.

LIST OF REFERENCES

1. Gustafson, A. J., and Calapodas, N. J., *Model 540 Rotor Blade Fatigue Test*, USAAMRDL Technical Note 22, Eustis Directorate, U.S. Army Air Mobility Research and Development Laboratory, Fort Eustis, Virginia, January 1976, AD A021472.
2. *Structural Analysis of 540-011-100-13 Hub and Blade Assembly for the Model 209/AH-1J, UH-1C, UH-1E, AH-1G, UH-1L, UH-1M, HH-1K Helicopters*, Report 209-099-174, Bell Helicopter Company, Fort Worth, Texas, November 1969.
3. *Qualification Load Level Survey for Improved Main Rotor for AH-1G*, Report 209-099-305, Bell Helicopter Company, Fort Worth, Texas, June 1970.
4. Forman, R. O., Kearney, V. E., and Engle, R. M., *Numerical Analysis of Crack Propagation in Cyclic-Loaded Structures*, Journal of Basic Engineering, September 1957.
5. Figge, I. E., and Newman, J. C., Jr., *Fatigue Crack Propagation in Structures With Simulated Rivet Forces*, ASTM Special Technical Publication No. 415, American Society for Testing and Materials, Philadelphia, Pennsylvania, September 1967.
6. Paris, P. C., and Sih, G. C. M., *Stress Analysis of Cracks*, ASTM Special Technical Publication No. 381, American Society for Testing and Materials, Philadelphia, Pennsylvania, June 1964.
7. Hudson, C. M., *Effect of Stress Ratio on Fatigue-Crack Growth in 7075-T6 and 2024-T6 Aluminum-Alloy Specimens*, NASA Technical Note D-5390, National Aeronautics and Space Administration, Washington, D. C., August 1969.
8. Hertzberg, R. W., *Deformation and Fracture Mechanics of Engineering Materials*, New York, John Wiley and Sons, 1976.

APPENDIX A CRACK PROPAGATION CALCULATIONS

L	L/r	$l(L/r)$	σ_0	$\sigma\sqrt{\pi a_0}$	$b_1 = a_0 + 0.25$	a/b	a/b_1	$F\left(\frac{a_0}{b_1}, \frac{a}{b}\right)$	$\frac{a_0}{b_0} F(l)^2$	$K = \frac{\sigma\sqrt{\pi a_0} F(l)}{(1-R)K}$	$\Delta K = \frac{\sigma\sqrt{\pi a_0} F(l)}{(1-R)K}$	da/dN	N_c
0.25	0.87	1.50	0.64	30348	0.89	2.11	0.70	1.20	0.92	36417	9470	1.65×10^{-6}	4.73×10^5
0.50	1.33	1.25	0.78	33504	1.03	1.97	0.66	1.24	1.20	41544	10803	2.65×10^{-6}	3.40×10^5
0.75	2.00	1.06	0.84	34768	1.09	1.91	0.64	1.25	1.31	43460	11302	3.15×10^{-6}	3.01×10^5
1.00	2.67	0.96	0.92	36386	1.17	1.83	0.61	1.28	1.51	46574	12111	4.09×10^{-6}	2.46×10^5
1.25	3.33	0.89	0.99	37745	1.24	1.76	0.59	1.29	1.64	48691	12662	4.87×10^{-6}	2.15×10^5
1.50	4.00	0.85	1.08	39424	1.33	1.67	0.56	1.32	1.88	52039	13533	6.35×10^{-6}	1.73×10^5
1.75	4.67	0.82	1.18	41208	1.43	1.57	0.52	1.35	2.15	53630	14466	8.39×10^{-6}	1.36×10^5
2.00	5.33	0.81	1.31	43419	1.56	1.44	0.48	1.38	2.50	59918	15582	1.16×10^{-5}	1.01×10^5
2.25	6.00	0.79	1.40	44886	1.65	1.35	0.45	1.43	2.86	64158	16684	1.59×10^{-5}	7.40×10^4
2.50	6.67	0.78	1.52	46770	1.77	1.23	0.41	1.45	3.20	67816	17636	2.09×10^{-5}	5.60×10^4
2.75	7.33	0.77	1.63	48433	1.88	1.12	0.37	1.50	3.67	72646	18892	3.02×10^{-5}	3.70×10^4

APPENDIX B
TEST LOAD AND CRACK GROWTH RECORD

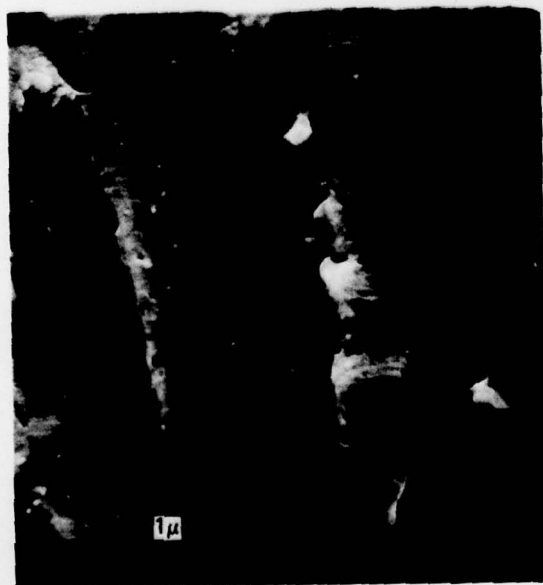
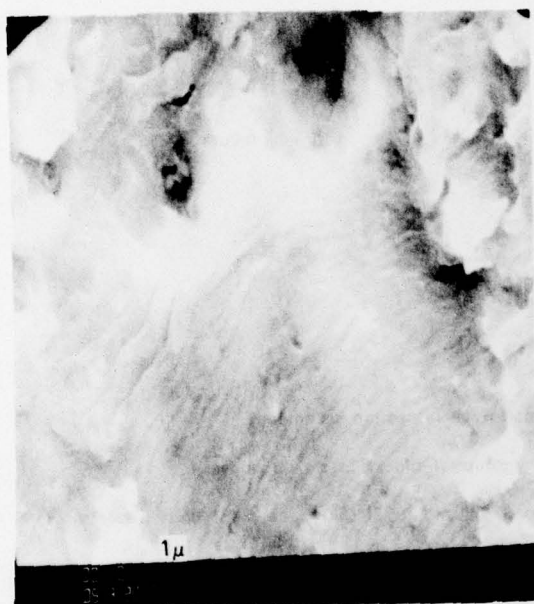
Load Block Number	Nominal Alternate Flap Bending (in.-lb)	Crack Propagation (in.)		Comments
		During Block	Total	
1	± 7,500	0	0	
2	± 7,500			
3	± 7,500			
4	± 11,000	0.15	0.25	Test load increased to initiate crack. Crack initiated, running to leading edge.
5	± 7,500	0.10	0.35	
6	± 7,500	0	0.35	
7	± 7,500	0	0.35	
8	± 7,500	0.19	0.54	
9	± 7,500	0	0.54	
10	± 7,500	0.03	0.57	
11	± 7,500	0.03	0.60	
12	± 7,500	0	0.60	
13	± 7,500	0.18	0.76	
14	± 7,500		0.76	
15	± 7,500	0.06	0.82	
16	± 7,500	0.06	0.88	
17,18	± 7,500	0.03	0.91	
19,20	± 7,500	0.10	1.01	
21,22	± 7,500	0.06	1.07	
23,24	± 7,500	0.12	1.19	
25,26	± 7,500	0.10	1.29	
27,28	± 7,500	0.10	1.40	
29,30	± 7,500	0.12	1.52	
31,32	± 7,500	0.12	1.64	

Load Block Number	Nominal Alternate Flap Bending (in.-lb)	Crack Propagation (in.)		Comments
		During Block	Total	
33,34	$\pm 7,500$	0.25	1.89	
35,36	$\pm 7,500$	0.25	2.14	
37,38				Continued running - no inspection.
39,40 41,42	$\pm 7,500$	0.71	2.85	
43	$\pm 7,500$	1.90	4.75	Ultimate failure.

NOTES:

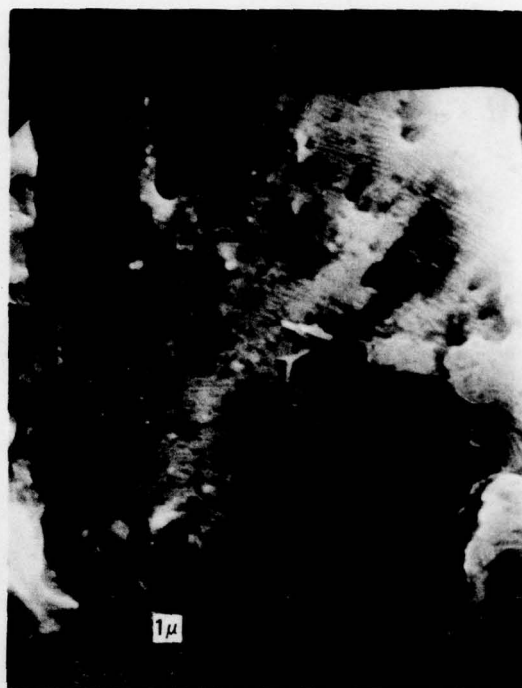
1. Steady axial load was nominally 76,000 pounds.
2. The load blocks consisted of 10,000 cycles each.
3. The crack growth was determined using ultrasonic shear wave inspection techniques.
4. The crack growth was determined after each block or group of blocks as shown above.
5. The alternating bending was removed and the axial load reduced to 30,000 pounds for each inspection.
6. Total crack propagation length shown includes 0.10-inch initial saw cut.

APPENDIX C
SCANNING ELECTRON FRACTOGRAPHS
OF FRACTURE SURFACE OF 540 ROTOR BLADE SPAR

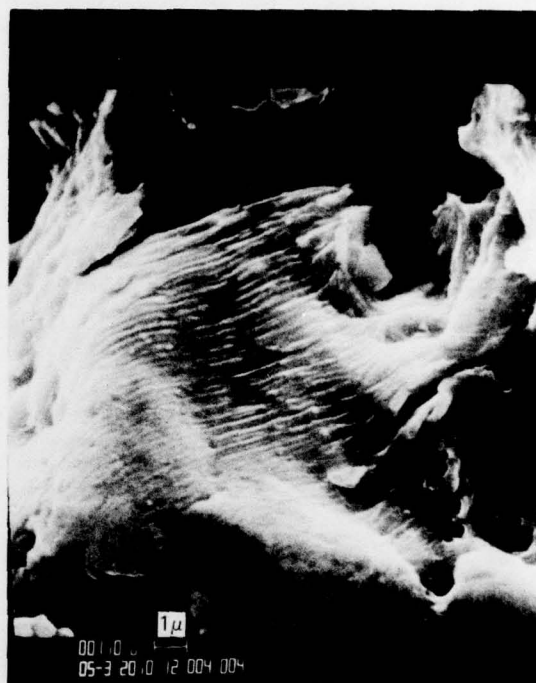


↑
Direction of crack growth

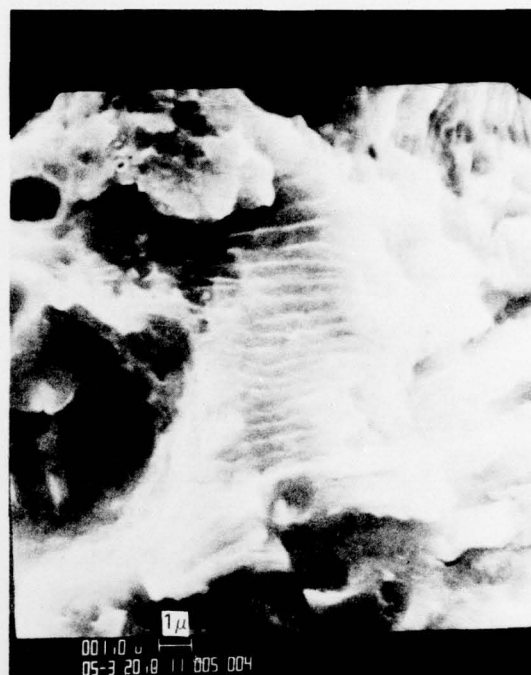
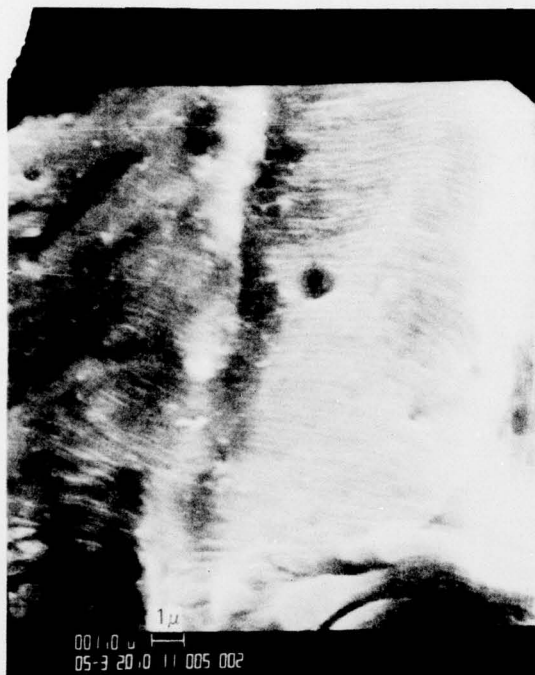
NOTE: The last two three-digit numbers on each fractograph are the section and location numbers identified in Figure 10.




↑
Direction of crack growth



Direction of crack growth




 Direction of crack growth

LIST OF SYMBOLS

a	=	half-crack length
a_e	=	effective half-crack length
\bar{a}_e	=	effective half-crack length
$f()$	=	a function of
ℓ	=	actual crack length
ℓ_c	=	critical actual crack length
ℓ_o	=	initial actual crack length
n	=	numerical exponent
r	=	radius
C	=	material constant
K	=	fracture mechanics stress-intensity factor
ΔK	=	stress-intensity-factor range
K_c	=	critical stress intensity factor for fracture
N	=	cycle number
N_o	=	initial cycle number
N_c	=	critical cycle number at crack instability
R	=	ratio, minimum stress to maximum stress
da/dN	=	crack extension per cycle of load
σ	=	applied stress normal to crack
$\Delta\sigma$	=	applied stress range